COMMISSARIAT À L'ÉNERGIE ATOMIQUE

DSM - DAPNIA

DIRECTION DES SCIENCES DE LA MATIÈRE

DEPARTEMENT D'ASTROPHYSIQUE, DE PHYSIQUE DES PARTICULES,
DE PHYSIQUE NUCLÉAIRE ET DE L'INSTRUMENTATION ASSOCIÉE

SERVICE D'ÉTUDE DES ACCÉLÉRATEURS

Nicolas PICHOFF

NOTE	
DATE : 11/09/98 N/RÉF. : DAPNIA/SEA 98/43	OBJET : **STATIONARY DISTRIBUTION OF SPACE-CHARGE DRIVEN CONTINUOUS BEAM** V/RÉF. :
DE : Nicolas PICHOFF	A : Jean-Michel LAGNIEL

STATIONARY DISTRIBUTION OF SPACE-CHARGE DRIVEN CONTINUOUS BEAM

Nicolas PICHOFF
Commissariat à l'Energie Atomique - DSM/DAPNIA/SEA
91191 Gif-sur-Yvette cedex. FRANCE.

Abstract

In a high intensity proton linac, the evolution of the beam distribution function is given by the Vlasov equation. The beam is in equilibrium in the channel when its distribution function f_0 is a stationary solution of the Vlasov equation. In that case, f_0 depends only on the Hamiltonian describing the particle movement. Six stationary distributions of unbunched beams have been analytically studied in a linear continuous focusing channel. It has been shown that:

- *Density profile of stationary distributions becomes uniform when the beam is space-charge dominated,*
- *Beam distribution in 2D phase-space becomes rectangular as space-charge increases.*

An expression of the beam border width has been found, and a model given the halo-particles trajectories in phase-space around a space-charge driven beam has been created.

Periodic (FODO) channels have been considered. Simulations have shown the good equivalence between periodic and continuous confinement channels in term of beam stationary distributions, emittance and halo evolution. An experiment in a FODO channel has exhibited the predicted results.

Contents

1. Theoretical basis (bunched and unbunched beams)

1.1 Stationary solutions of the Vlasov Equation

When the effects of binary coulombian collisions between particles can be neglected in the beam dynamics, its distribution function $f(\vec{r},\vec{p},t)$ evolution is described by the Vlasov equation :

$$\frac{\partial f}{\partial t}+\frac{\vec{p}}{\gamma m}\cdot\vec{\nabla}_{\vec{r}}f+\vec{F}(\vec{r},t)\cdot\vec{\nabla}_{\vec{p}}f=0\,. \qquad \textbf{(Eq. 1)}$$

$\vec{r}$ is the position, $\vec{p}$ the momentum of the particle, γm its relativistic mass,

$\vec{F}(\vec{r},t)$ is the force acting on particle at position $\vec{r}$ and time t. This force is the sum of the external confinement force F_c and the space-charge forces F_{sc}. We will consider it can be derived from a potential and then does not depend on $\vec{p}$.

The beam is in equilibrium in a continuously focusing channel (its distribution function does not depend on time) if :

$$\frac{\partial f_0}{\partial t}=0 \qquad \Leftrightarrow \qquad \frac{\vec{p}}{\gamma m}\cdot\vec{\nabla}_{\vec{r}}f_0+\vec{F}(\vec{r},t)\cdot\vec{\nabla}_{\vec{p}}f_0=0\,. \qquad \textbf{(Eq. 2)}$$

The hamiltonian describing the movement of a particle in the stationary potential well ϕ is then :

$$H=c\cdot\left(m^2c^2+p_x^2+p_y^2+p_z^2\right)^{\frac{1}{2}}+q\cdot\phi(x,y,z), \qquad \textbf{(Eq. 3)}$$

$\phi=\phi_c+\phi_{sc}$, is the sum of the contribution of the external confinement potential ϕ_c and this of the space-charge potential ϕ_{sc}.

The hamiltonian can be written as :

$$H=E_k\left(p_x,p_y,p_z\right)+W_c(x,y,z)+W_{sc}(x,y,z). \qquad \textbf{(Eq. 4)}$$

E_k being the kinetic energy of the particle,
W_c the confinement potential energy,
W_{sc}, the space-charge potential energy.

The beam distribution function f_0 does not depend on time if it depends explicitly on the hamiltonian :

$$f_0(\vec{r},\vec{p})=F_0\left(H(\vec{r},\vec{p})\right). \qquad \textbf{(Eq. 5)}$$

The beam distribution is stationary if the isodensity-curves in the phase-space (contour-plot of the beam) correspond to the iso-hamiltonian curves which are the trajectories of the particles in the phase-space. If you look at a small volume $(d\vec{r}, d\vec{p})$ of the phase-space, the number of particles moving out of this volume, during the time dt, equal the number of particles entering it.

1.2 Charge density equivalent to a confinement force

The non relativistic Newton equation is :

$$\frac{d\vec{p}}{dt} = m \cdot \frac{d^2\vec{r}}{dt^2} = \vec{F}(\vec{r}, \vec{p}, z), \qquad \textbf{(Eq. 6)}$$

m being the protons mass.

If the dependence of the force $\vec{F}$ on the beam momentum dispersion can be neglected ($\vec{F}$ depends only on the position), it is equivalent to a confinement electric field $\vec{E}$:

$$\vec{E}(\vec{r}, z) = \frac{\vec{F}(\vec{r}, z)}{q}, \qquad \textbf{(Eq. 7)}$$

q being the beam-particle charge.

The relationship between a charge density and an electric field is given by the Gauss Law :

$$\vec{\nabla} \cdot \vec{E}(\vec{r}, z) = \frac{\rho(\vec{r}, z)}{\varepsilon_0}, \qquad \textbf{(Eq. 8)}$$

The confinement force felled by the beam particles is then the one induced by an opposite charge distribution of density :

$$\boxed{n(\vec{r}, z) = \frac{\varepsilon_0 \cdot \vec{\nabla} \cdot \vec{F}(\vec{r}, z)}{q^2}}, \qquad \textbf{(Eq. 9)}$$

In a continuous, linear focusing channel with a phase advance per meter k_0 :

$$n(\vec{r}) = n_0 = \frac{4 \cdot \varepsilon_0}{q^2} \cdot E_k \cdot k_0^2, \qquad \textbf{(Eq. 10)}$$

E_k is the beam-particle kinetic energy.

1.3 Stationary density profile and phase-space shape of highly depressed beam

The evolution of the beam envelope R is described by the equation [1]:

$$d^2R/dz^2 + F_c(R) - F_{sc}(\Re) - \varepsilon_R^2/R^3 = 0 ,$$

where R and ε_R stand for the beam-envelope radius and emittance, respectively, in the three spatial directions, X, Y, Z, and $\Re$ is a function of the transverse sizes (X and Y) for a continuous beam, and of the three sizes (X, Y and Z) for a bunched beam. $F_c(R)$ denotes the confinement force, and $F_{sc}(\Re)$ the space-charge force.

In the case of a matched beam ($d^2R/dz^2 = 0$), the particle distribution is stationary with $R = R_m$.

We consider the parameter $\zeta_R = F_{sc}(\Re_m) \cdot R_m^3 / \varepsilon_R^2$ which is the ratio between the space-charge force and the emittance force acting on the beam. It is related to the tune depression factor η_R by:

$$\zeta_R = \eta_R^{-2} - 1 . \qquad \textbf{(Eq. 11)}$$

If $\zeta_R >> 1$ $(\eta_R << 0.7)$, the beam is space-charge dominated.

If $\zeta_R << 1$, the beam is emittance dominated. Let us examine these two cases.

- $\zeta_R << 1$. The contribution of the space-charge potential energy to the hamiltonian can be neglected. We have $H(\vec{r},\vec{p}) \approx E_k(\vec{p}) + W_c(\vec{r})$. If external confinement is linear in all directions, the particle potential energy is proportional to r^2 and, as the particle kinetic energy is proportional to p^2, all beam particles are moving in a harmonic potential well and the iso-density curves are ellipses in the phase sub-spaces. The stationary beam profile depends on the initial density distribution.
- $\zeta_R >> 1$. To maintain beam confinement, the focusing force must oppose the large repulsive space-charge force. Since $|W_c(\vec{r})|, |W_{sc}(\vec{r})| >> |H(\vec{r},\vec{p}) - E_k(\vec{p})|$, we have :

  $$W_{sc}(\vec{r}) \underset{\eta_R \to 0}{\to} - W_c(\vec{r}) . \qquad \textbf{(Eq. 12)}$$

  If external confinement is linear in all directions, so is the space-charge force, and the stationary particle distribution inside the beam is homogeneous. For increasing intensities, beam particles are moving in a potential well which is no longer harmonic but becomes flater and flater in the central region of the beam and has a sharp increase at the beam boundary. This is a "reflective-wall potential" since the particles do not feel any force inside the beam, move freely with constant momentum and are reflected at the boundary. The phase-space distribution becomes rectangular.

2. Unbunched beam

2.1 Continuously focusing channel

The external confinement force does not depend on z. It is assumed being the same in the horizontal and in the vertical direction.

2.1.1 Stationary solution of the Vlasov-Maxwell system

2.1.1.1 Potential well and beam density calculation

The transverse momentum is :

$$p_\perp^2 = p_x^2 + p_y^2 .$$

Most of the time, $p_\perp << p_z$, and the hamiltonian of unbunched beam becomes :

$$H = \gamma mc^2 + \frac{p_\perp^2}{2 \cdot \gamma m} + q \cdot \phi(x,y,z). \qquad \textbf{(Eq. 13)}$$

Since the transverse and longitudinal movements are uncoupled, the hamiltonian of the transverse movement can be written :

$$H_\perp = \frac{p_\perp^2}{2 \cdot \gamma m} \cdot + q \cdot \phi(x,y) \cdot g(z). \qquad \textbf{(Eq. 14)}$$

Dividing (Eq. **14)** by γmv^2, $v = \beta c$ being the speed of the particle-beam, we will define the hamiltonian as :

$$H_\perp = \frac{1}{2} r_\perp'^2 + \frac{q \cdot \phi(x,y)}{\gamma mv^2} g(z), \qquad \textbf{(Eq. 15)}$$

with $r_\perp'^2 = x'^2 + y'^2 = \left(\frac{p_\perp}{\gamma mv} \right)^2 .$

For a beam in equilibrium in an axisymetric continuous focusing channel :

$$H_\perp = \frac{1}{2} r_\perp'^2 + \frac{q \cdot \phi_c(r)}{\gamma mv^2} + \frac{q \cdot \phi_{sc}(r)}{\gamma^3 mv^2} = \frac{1}{2} r_\perp'^2 + W(r), \qquad \textbf{(Eq. 16)}$$

with $r^2 = x^2 + y^2$,

ϕ_c and ϕ_{sc}, the confinement and electrostatic space-charge potential,

W(r), the total potential energy of the beam,

$\frac{1}{2} r_\perp'^2$, its normalised kinetic energy,

the γ^3 factor comes from the magnetic compensation of the electrostatic force (divided by γ^2) when relativistic.

It can be shown [5] that :

$$\boxed{n(r) = 2\pi \int_{W(r)}^{W(a)} f(H_\perp) \cdot dH_\perp}, \qquad \textbf{(Eq. 17)}$$

from which the potential-well shape can be obtained by solving the Poisson equation :

$$\boxed{\frac{1}{r}\frac{d}{dr}\left(r\frac{d\phi_{ce}}{dr}\right)=-\frac{q\cdot n(r)}{\varepsilon_0}=-\frac{2\pi q}{\varepsilon_0}\int_{W(r)}^{W(a)} f\left(H_\perp\right)\cdot dH_\perp}. \qquad \textbf{(Eq. 18)}$$

From these last two equations, both potential well and beam radial density profile can be solved numerically for different hamiltonian distribution functions $f(H_\perp)$.

2.1.1.2 Results in a linear confinement force over six different hamiltonian distributions

In **Table 1**, have been summarised the 6 different hamiltonian dependence of the distributions function f(H) studied in this paper. f(H) has been set to 0 for $|H| > H_0$.

	Maxwell-Boltzman	**Gaussian**	**Linear-Decreasing**
f(H)	$K_0\cdot\exp\left(-\frac{H}{H_0/5}\right)$	$K_0\cdot\exp\left(-\left(\frac{H}{H_0/2}\right)^2\right)$	$K_0\cdot\left(H_0-H\right)$
$\Gamma=\sigma_\infty/\sigma_2$	3.77	2.89	2.37
	Parabola	**Water-Bag**	**Linear-Increasing**
f(H)	$K_0\cdot\left(H_0^2-H^2\right)$	K_0	$K_0\cdot H$
$\Gamma=\sigma_\infty/\sigma_2$	2.17	1.73	1.414

Table 1 : The 6 studied distributions

We have defined : $\sigma_n=\left(\frac{1}{I}\cdot\int_0^{H_0} f(H)\cdot H^n\cdot dH\right)^{\frac{1}{n}}$ the distribution momentum of order H, with $I=\int_0^{H_0} f(H)\cdot dH$. $\Gamma=\sigma_\infty/\sigma_2$ is giving an idea of the shape of the distribution: The higher Γ is, the more intense is the distribution for small energy. The shape of these distributions can be shown in the **Figure 1**.

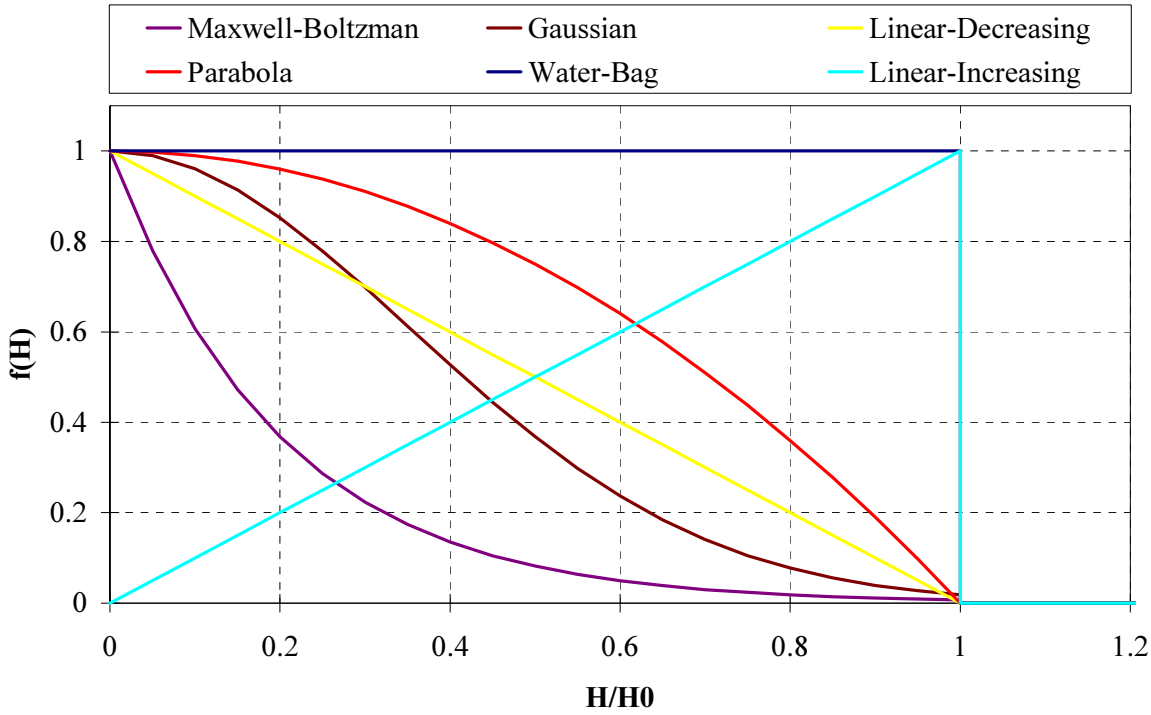

Figure 1 : The 6 studied distributions

2.1.1.2.1 Beam density profile

By solving numerically **(Eq. 18)** and **(Eq. 17)**, we have calculated the equilibrium density profile of these 6 beams with different depressed-tune factors : 1, 0.8, 0.6, 0.4, 0.275. They are represented on **Figure 2**. The radius has been normalised to the total beam radius, the profile has been normalised to the beam-centre profile. It appears clearly that the beam density profile becomes flatter and flatter (homogenous) as the beam current increases whatever the hamiltonian distribution.

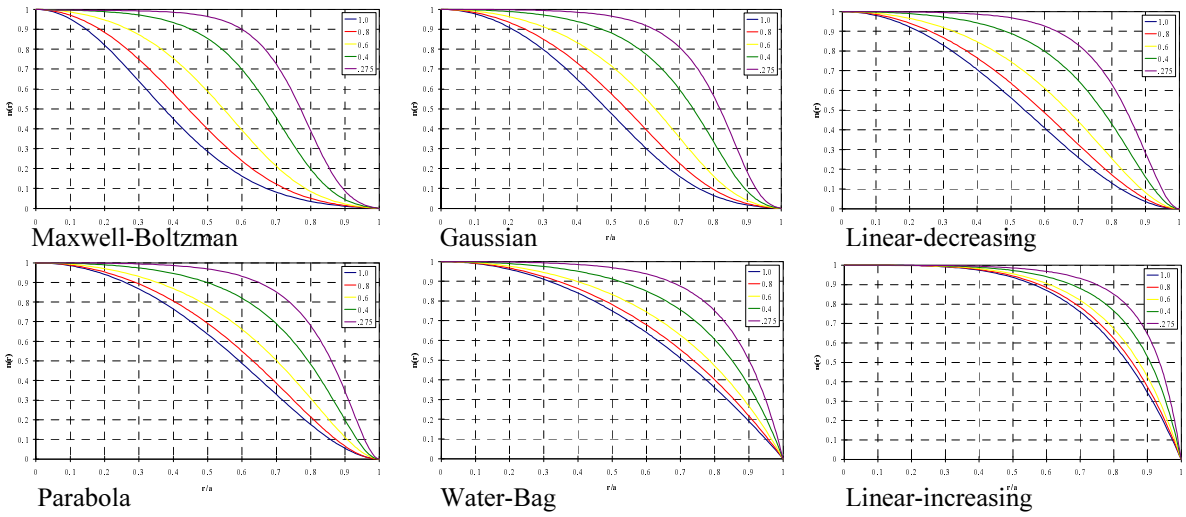

Figure 2 : Equilibrium density profile for different beams at various depressed tunes.

The density profile at the beam centre reaches a maximum value when the tune depression is very large (**Figure 3**). This density value corresponds to the one equivalent to the external focusing which has been calculated from **(Eq. 10)** to 1.105 10^{14} m^{-3}. This is coherent with **(Eq. 12)** which says that at high space-charge depression, the space charge potential is close to the confinement one, leading to a beam density close to the confinement-equivalent density.

We have multiplied the focusing phase advance per meter k_0 by a factor 2 (multiply the force $\left(F(r) = -k_0^2 \cdot r\right)$ by a factor 4), and we have observed that the central density is then multiplied by a factor 4 (**Figure 4.a**).

For high space-charge depression, the beam size varies in $1/k_0$.

We can do some remarks about the beam edges :

- For the same external confinement force (or beam density), the beam-edge width seems to be the same whatever the space-charge depression (if lower than 0.5) (**Figure 3**).
- The beam-edge width is moving in 1/a (**Figure 4.b**), $1/k_0$ or $1/\sqrt{n_0}$, n_0 being the density equivalent to the external confinement force. In the case of the **Figure 4**, the plasma length at the beam centre has been estimated to 0.5 mm. This plasma length dependence with n_0 is the same that this observed for the edge width ($\propto 1/\sqrt{n_0}$). That is why many authors have considered that the beam-edge width can then be estimated to a few plasma length.

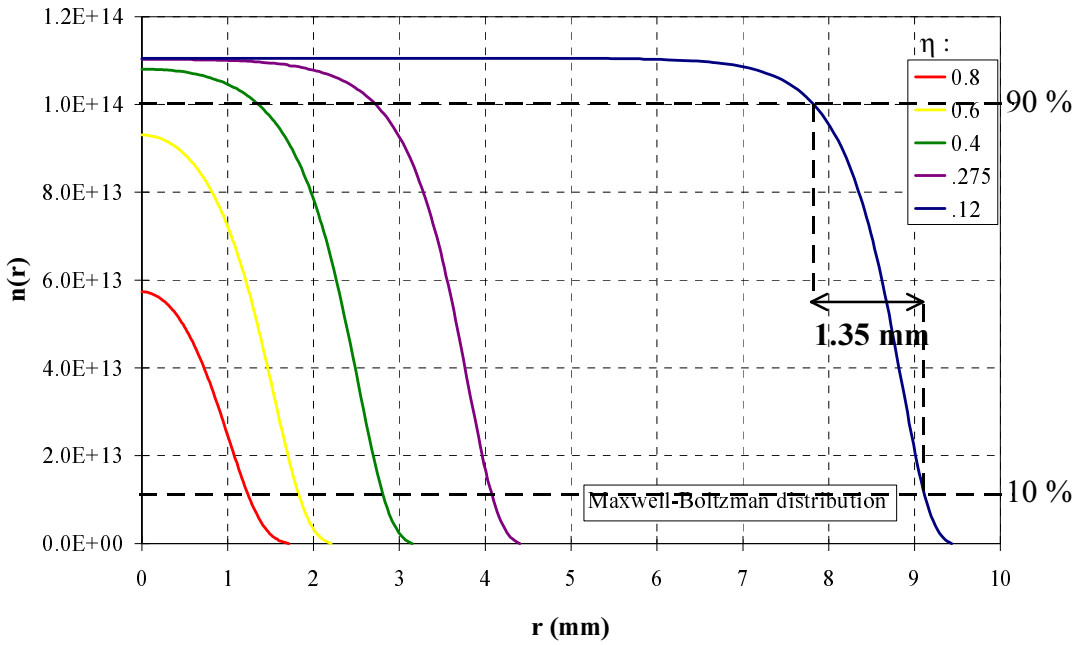

Figure 3 : Density profile of a Maxwell-Boltzman distribution for various depressed tune

The beam-edge width has beam estimated to 1.35 mm.

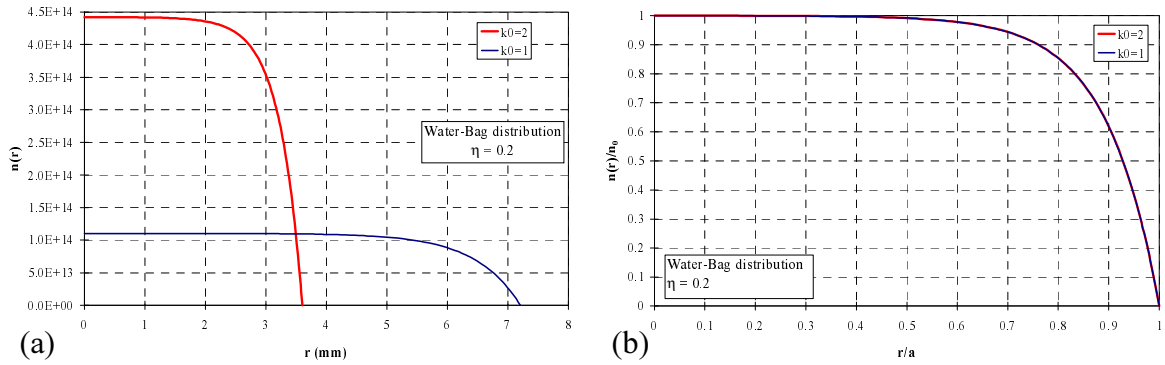

Figure 4 : Effect of the confinement force on the beam-centre density, the beam size and the edge-width in an highly depressed beams for 2 different external focusing force.

Left (a) : not normalised,

Right (b) : normalised to the full size and the maximum density.

We have an other interpretation, based on a simple model, in order to calculate the beam-edge width :

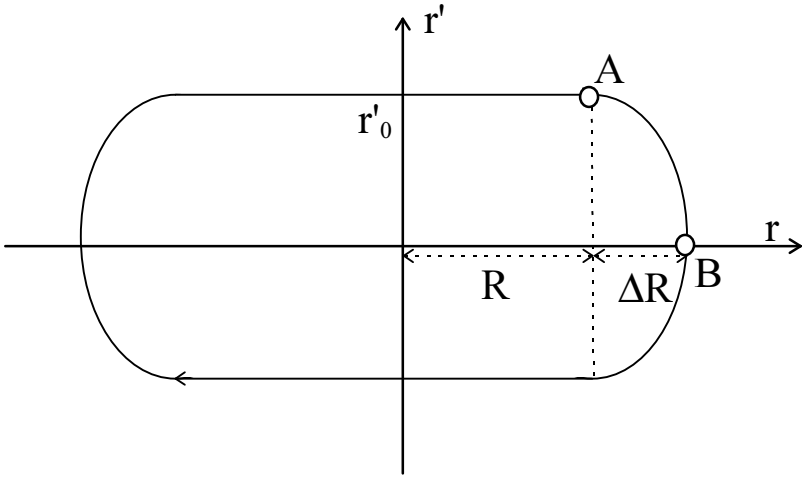

Figure 5 : Particle trajectory in a highly depressed beam

On **Figure 5**, has been represented the trajectory, in the phase space, of an outermost particle of a space-charge dominated beam. In order to calculate the maximum amplitude R+ΔR of this particle of energy H_0, we use the energy conservation principle between points A and B on **Figure 5**. We have the relationship :

$$\frac{1}{2}r_0'^2 = \left(\frac{1}{2}k_0^2\cdot(R+\Delta R)^2 - K\cdot\ln(R+\Delta R)\right) - \left(\frac{1}{2}k_0^2\cdot R^2 - K\cdot\ln(R)\right), \qquad \textbf{(Eq. 19)}$$

which gives :

$$r_0'^2 = k_0^2\cdot\Delta R\cdot R\left(2+\frac{\Delta R}{R}\right) - K\cdot\frac{\Delta R}{R}, \qquad \textbf{(Eq. 20)}$$

having assumed $\Delta R/R << 1$, and $\ln(1+\varepsilon)\approx\varepsilon$.

with $K = (1-\eta^2)\cdot k_0^2\cdot R^2$, we have :

$$r_0'^2 = k_0^2\cdot\Delta R\cdot R\left(\eta^2+\frac{\Delta R}{R}\right). \qquad \textbf{(Eq. 21)}$$

The solution of this second order equation gives, with $r_0'^2 = 2\cdot H_0$:

$$\boxed{\frac{\Delta R}{R} = \frac{\sqrt{\eta^4 + \dfrac{8\cdot H_0}{k_0^2\cdot R^2}} - \eta^2}{2}}. \qquad \textbf{(Eq. 22)}$$

If $\dfrac{8\cdot H_0}{k_0^2\cdot R^2} >> \eta^4$, we get : $\boxed{\Delta R = \sqrt{\dfrac{2\cdot H_0}{k_0^2}}}$. **(Eq. 23)**

.

In that case, with H_0 constant, the edge-width does not depend on the depressed-tune (see **Figure 3**), and as the equilibrium beam size R is proportional to k_0^{-1}, $\Delta R/R$ is the same whatever the confinement force (see **Figure 4.b**).

In the numerical resolutions presented on **Figure 3**, we have $H_0 = 10^{-6}$, $k_0 = 1\ m^{-1}$, R greater than 2 mm and η lower than 0.4. We verify that $\frac{8 \cdot H_0}{k_0^2 \cdot R^2} >> \eta^4$. In these conditions, **(Eq. 23)** gives $\Delta R = 1.4$ mm which can be compared to the edge width estimated to 1.35 mm on **Figure 3**.

2.1.1.2.2 Phase-space distribution

In order to understand the evolution of the beam phase-space distribution with depress tune, the potential well in the beam has been calculated and represented on **Figure 6**. As the density profile, it becomes flater and flater with the increasing space-charge forces. When the depressed tune is close to 0, it becomes a reflecting wall.

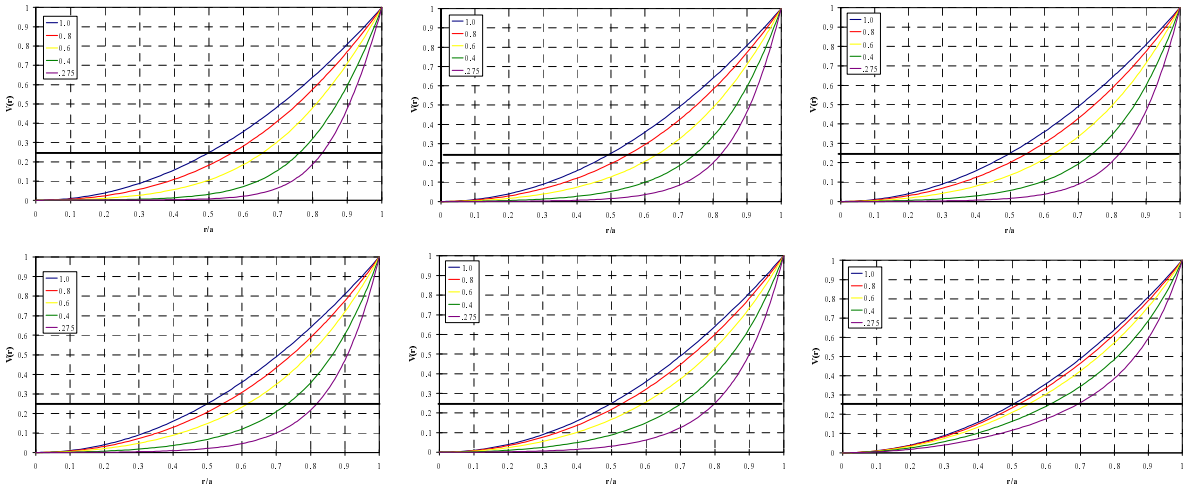

Figure 6 : Confinement potential well in beams in equilibrium

On **Figure 7**, are represented 2 particles trajectories in the gaussian beam for different tune depressions. The 2 particles have respectively the maximum energy of the beam (H_0), and one fourth of this energy ($H_0/4$). The trajectories are ellipses when there is no space-charge forces (and linear external force), and becomes more and more rectangular with a decreasing η.

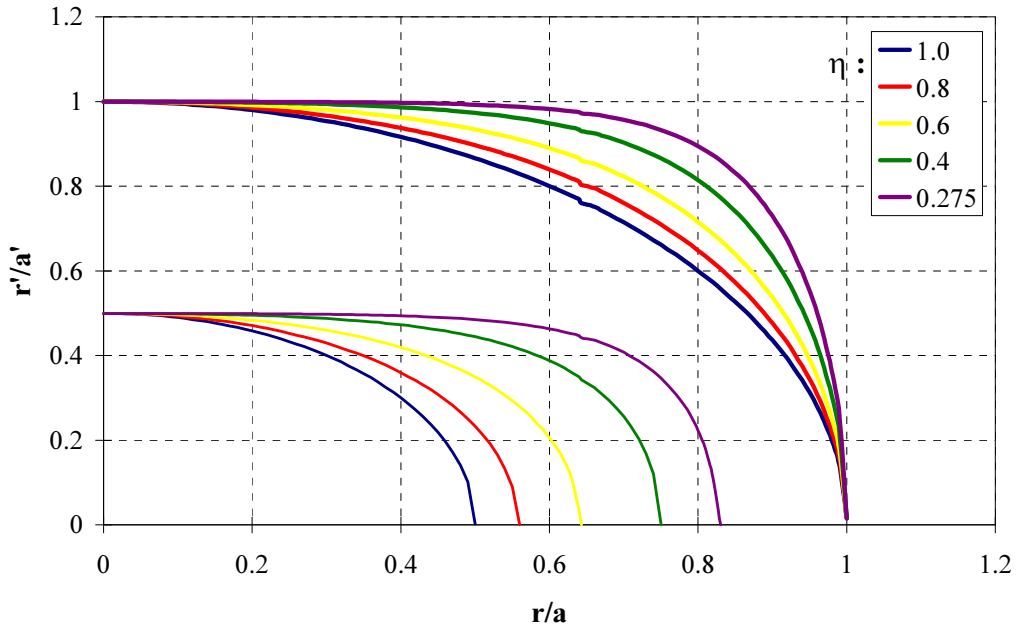

Figure 7 : Particle trajectories (iso-hamiltonian curves) in the phase space

In order to quantify the evolution of the beam-phase space distribution with the space-charge, we define a new parameter α as being 2 times the amplitude (normalised to the beam size) of the particle of energy $H_0/4$. This parameter, which quantify the aspect ratio of the beam in the phase-space, equals 1 when there is no space-charge force and tends to 2 when the beam is space-charge dominated. On **Figure 8**, have been represented the evolution of α with η for the six hamiltonian distributions. For each distribution, we note that the maximum hamiltonian value for a beam-particle is H_0. The curve-shape is dependant on the Γ parameter :

- When $\Gamma >> 1$, the curve $\alpha(\eta)$ tends to a strait line: $\alpha = 2 - \eta$,
- When $\Gamma \rightarrow 1$ (K-V beam), the curve $\alpha(\eta)$ tends to a strait line: $\alpha = 1$.

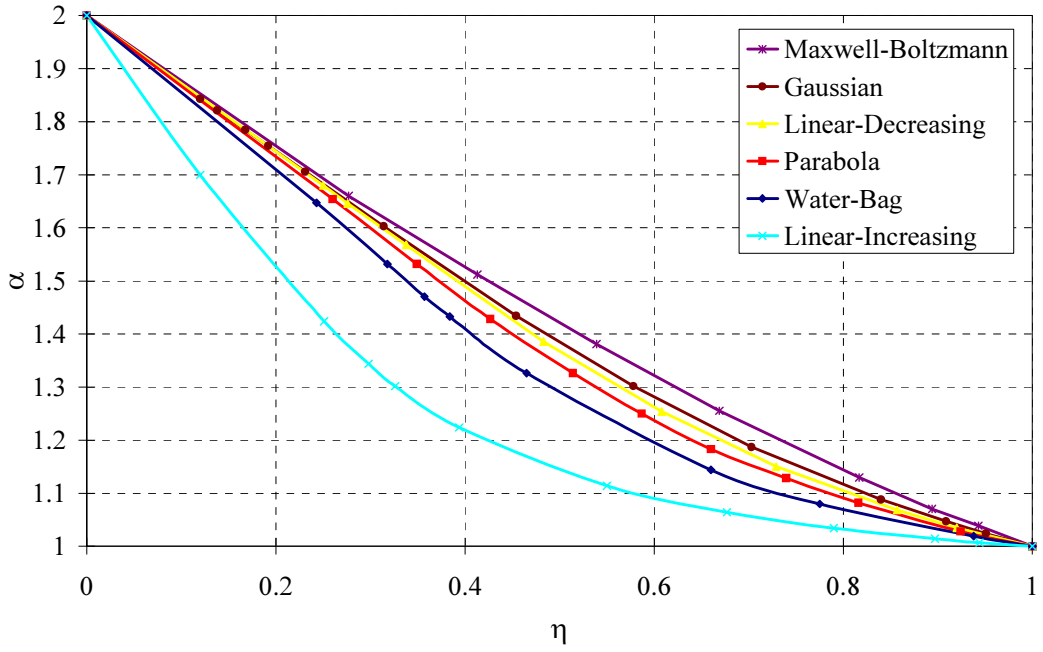

Figure 8 : Evolution of the aspect ratio α of beam in phase-space with depress tune η

2.1.1.2.3 Model of particle trajectories around a space-charge driven beam

Magnitude of physical effects (like intrabeam scattering [2] or beam scattering on residual gas [3]) on halo density is often easier calculated without taking into account the space-charge forces. It should be very interesting to extrapolate these results by taking into account the space charge force. We will then create a rough model giving a particle trajectory in phase-space around space-charge driven beam. The model basis is the same as this used to calculate beam edge width (**Figure 5**) :

- Particle does not feel any force for $r < R$ with $R = (1-\eta)\times r_0$, r_0 being the maximum beam-core radius.
- Particle feels only external force ($=k_0 \times r$) for $r > R$.

Particle trajectory is then :

$$\begin{cases} r' = r'_m & \text{if } r < R \\ k_0^2 \cdot (r - R)^2 + r'^2 = r'^2_m & \text{if } r \geq R \end{cases} \qquad \textbf{(Eq. 24)}$$

On , we have represented the trajectories of halo particles around a Water-Bag beam and those obtained with the model. The depress-tune goes from 1 to 0.2. On , has been represented the halo-particle trajectories around 3 different beam (Maxwell-Boltzman, linear decreasing and Water-Bag) and those obtained with the model for $\eta = 0.2$. The model seems to be a good mean choice between all the trajectories.

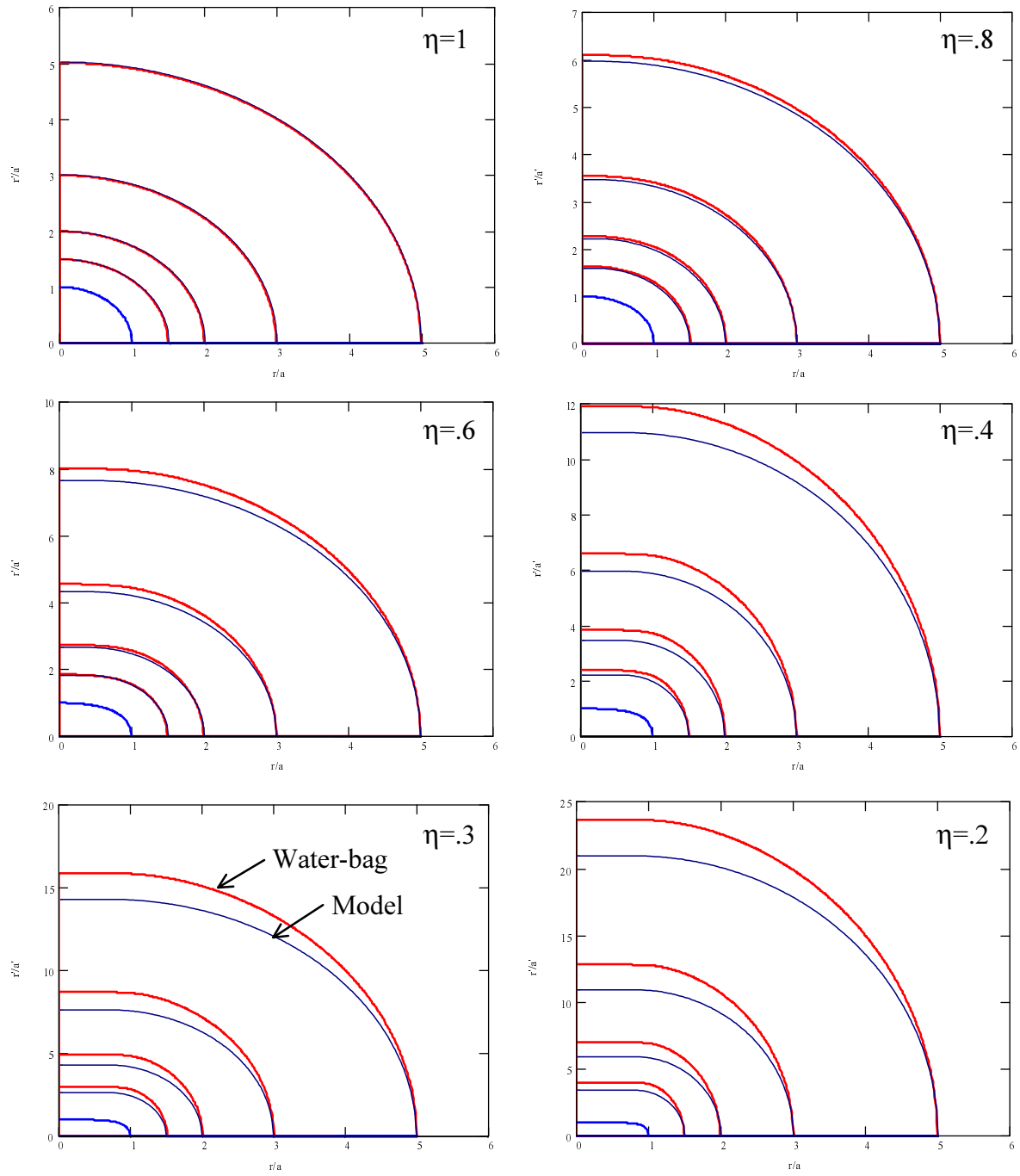

Figure 9 : Halo particle trajectories

- around a Water-Bag beam (red),
- found with the model (blue).

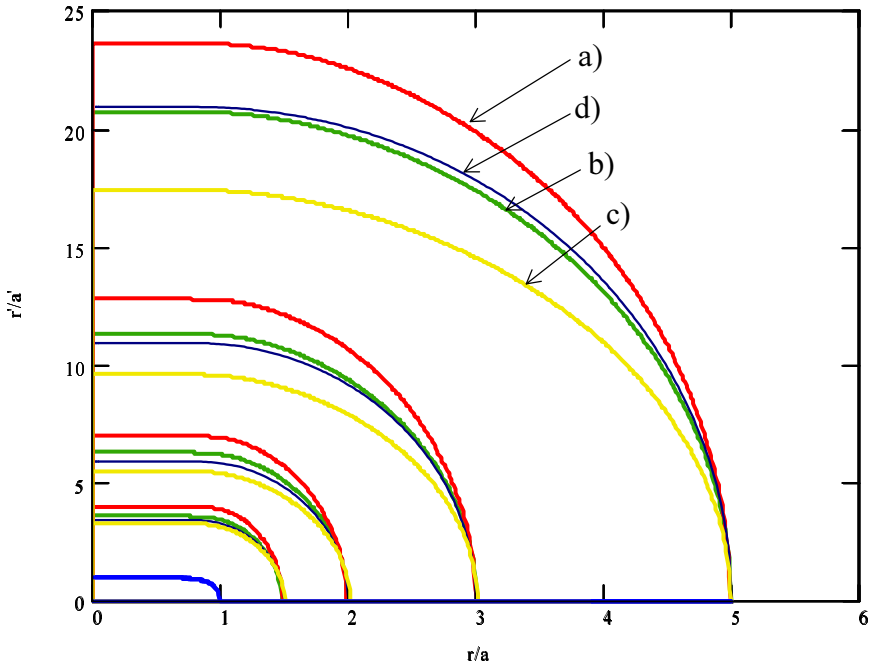

Figure 10 : Halo-particle trajectories for η=0.2

- a) Water-Bag beam (red),
- b) Linear decreasing beam (green),
- c) Maxwell-Boltzman beam (yellow),
- d) Model (bleu).

2.1.1.3 Beam in a non linear confinement force

Modelisation of non linear confinement force has been done with the potential :

$$U(r) = \frac{1}{2} k_0^2 \cdot r^2 + \frac{1}{4} B \cdot r^4 . \qquad \textbf{(Eq. 25)}$$

In the linear channel, B=0 (and k_0=1 m^{-1}). Now we will study the two cases with B=4000 (over-focusing) and B=-4000 (under-focusing). The distribution studied is the Water-Bag distribution.

2.1.1.3.1 Over-focused beam

On **Figure 11**, has been represented the beam density profile, for different currents, in the over-focusing channel. The negatively-charged density distribution equivalent to this channel calculated with **(Eq. 9)** has been represented. As predicted before, the beam density profile tends to this distribution as the space-charge increases.

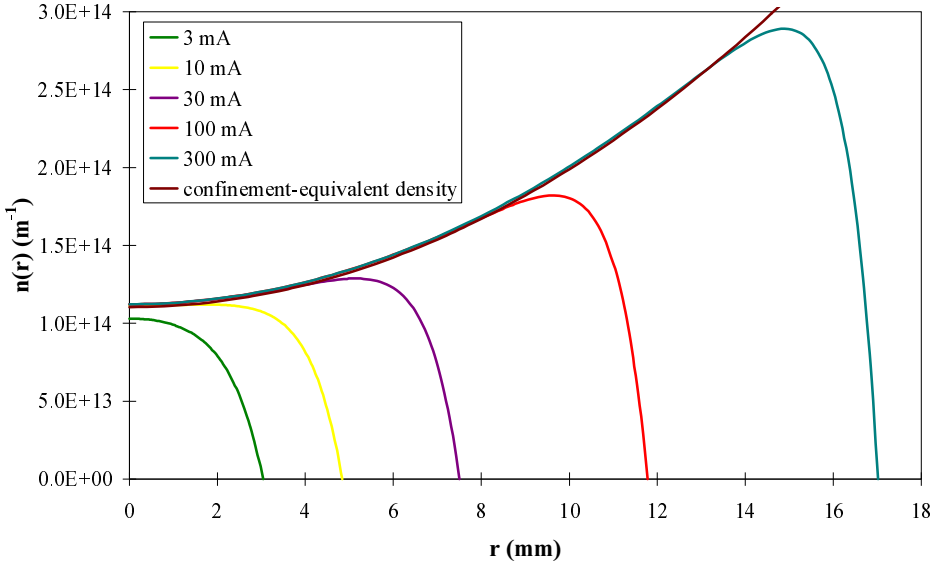

Figure 11 : Beam density profiles in an over-focusing channel

2.1.1.3.2 Under-focused beam

On **Figure 12**, has been represented the beam density profile, for different currents, in the under-focusing channel. The negatively-charged density distribution equivalent to this channel calculated with **(Eq. 9)** has been represented. As predicted before, the beam density profile tends to this distribution as the space-charge increases. In that case, the maximum beam current which can be transported is 33 mA.

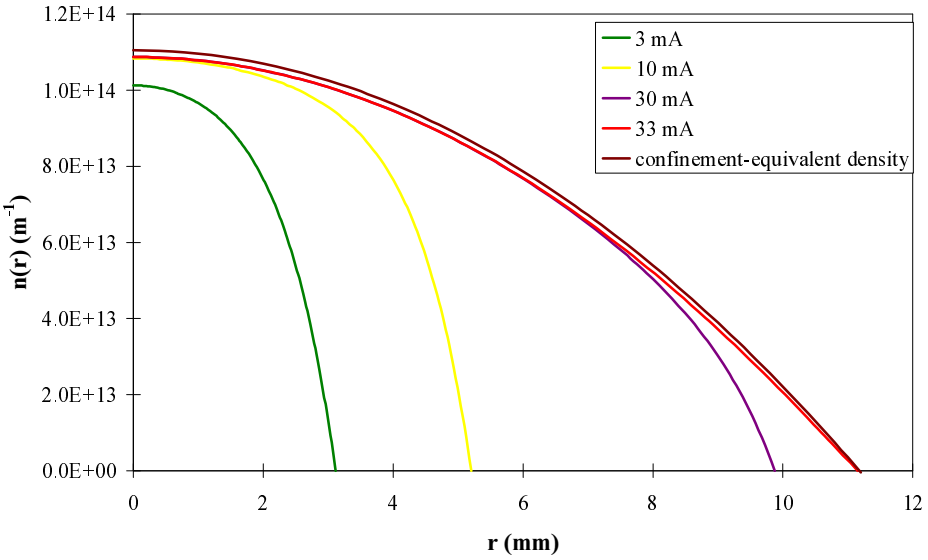

Figure 12 : Beam density profiles in an under-focusing channel

2.1.2 Particle in Cells simulations

2.1.2.1 The simulation program

The goals of these simulations are :

- to verify the agreement between 1D analytical predictions and 2D numerical particle in cell simulations.
- to explore the difference between a periodic focusing channel and its equivalent continuous one. This will give an estimation of the validity of analytic predictions even in a periodic focusing channel.
- to study the process of redistribution toward stationary distribution.

Simulations have been done with MONET [4] code dedicated to the dynamics of continuous beams. Thre different channels have been used :

- A continuous focusing channel with a phase-advance per meter (without space-charge) $k_0 = 1\ m^{-1}$.
- A FODO channel with a phase advance per period (without space-charge) $\sigma_0 = 60°$, a period length $L = \frac{2 \cdot \pi}{6}$ which gives a phase-advance per meter $k_0 = 1\ m^{-1}$. The Drift and quadrupole length is L/4.
- A FODO channel with a phase advance per period (without space-charge) $\sigma_0 = 80°$, a period length $L = \frac{4 \cdot \pi}{9}$ which gives a phase-advance per meter $k_0 = 1\ m^{-1}$. The Drift and quadrupole length is L/4.

Beams, with depress tunes η between 0.1 and 1, have been RMS-matched to the channels with envelope code. They have all the same initial RMS-emittance. The initial beam phase-space distribution is always gaussian[1] :

$$n(x,x',y,y') = n_0 \cdot \exp\left[-\frac{1}{2}\left(\left(\frac{x}{\sigma_x}\right)^2 + \left(\frac{x'}{\sigma_{x'}}\right)^2 + \frac{x \cdot x'}{\sigma_{xx'}} + \left(\frac{y}{\sigma_y}\right)^2 + \left(\frac{y'}{\sigma_{y'}}\right)^2 + \frac{y \cdot y'}{\sigma_{yy'}}\right)\right],$$

The σ values are calculated from the Twiss parameters of the RMS-matched beam.

2.1.2.2 Beam density profile

Final beam-density profiles have been represented on **Figure 13**. They exhibit a density-profile becoming more and more homogenous as the current increases. As analytically predicted, the central density of a space-charge dominated beam reaches the one equivalent to the confinement force.

[1] This means that the beam is not initially in equilibrium in the channel.

With small depress tune, the tail shape seems to have an exponential slope rather than gaussian as it is at low current.

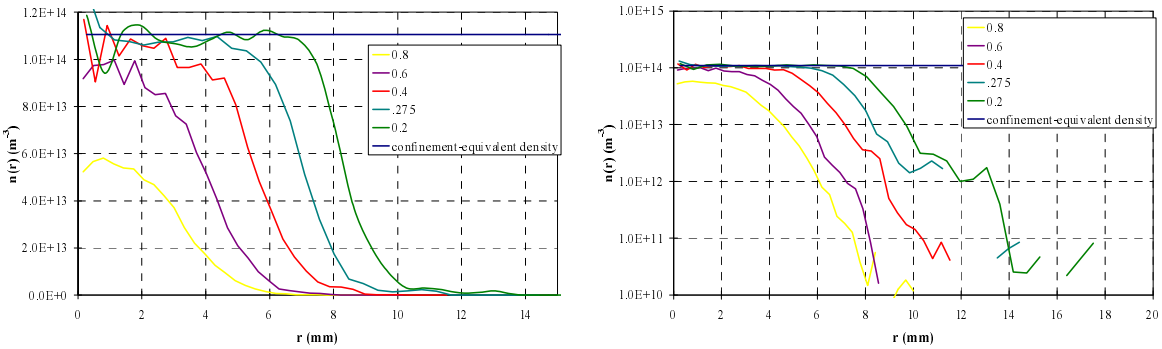

Figure 13 : Beam density-profiles at the end of the continuous channel
Left : Linear scale. Right : Logarithm scale.

2.1.2.3 Phase-space distribution

The phase-space distribution (contour-plot) of the beams at the exit of the continuous channel have been represented on **Figure 14**. The lines correspond to density from 1 % to 81 % with 10 % step. As shown in **Figure 7**, phase-space distribution becomes more and more rectangular as the beam current increases.

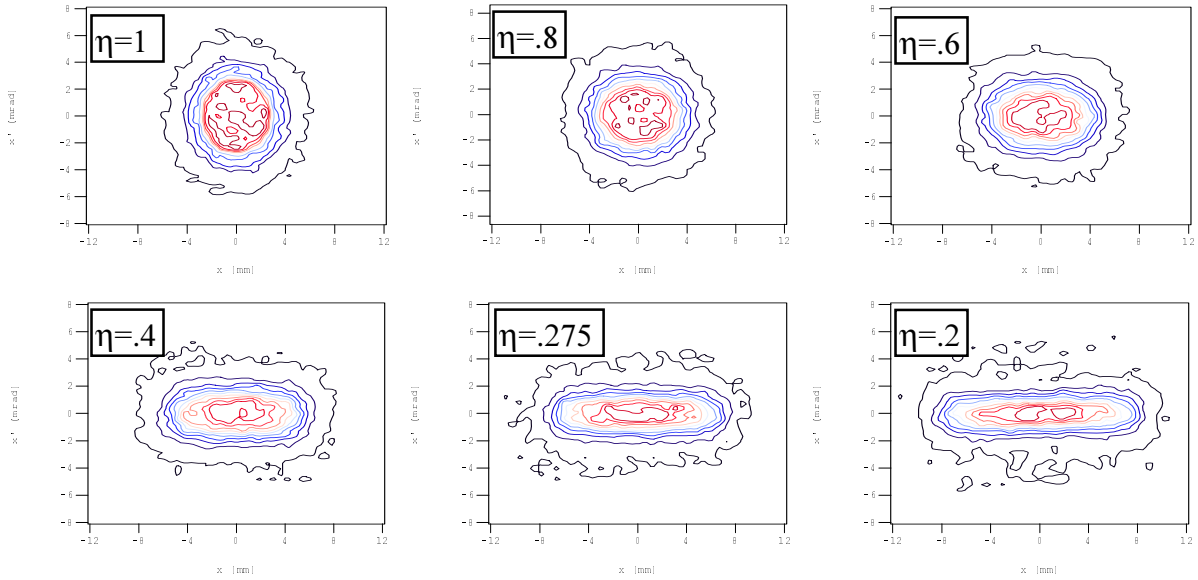

Figure 14 : Beam distribution in (x,x') phase-space at the end of a 20 meters uniform focusing channel for different tune depression.

Evolution of the aspect ratio α of the beam in the continuous focusing channel has been studied. Results are presented in **§ 2.2.2** (**Table 2**, **Figure 20**), in order to be compared to those obtained in a FODO channel.

2.1.2.4 Evolution toward this equilibrium

As previously mentioned, the initial 4D gaussian beam is not in equilibrium at the channel input. This beam evolves quickly toward an equilibrium at the beginning of the transport.

This evolution induced an emittance growth, represented on **Figure 15**. We have represented the relative emittance growth, along the channel, of RMS-matched beams with depressed-tune from 0.1 to 0.9. The relative emittance growth is defined as : $\frac{\varepsilon_f - \varepsilon_i}{\varepsilon_i}$, ε_f and ε_i being respectively the final and the initial beam emittance.

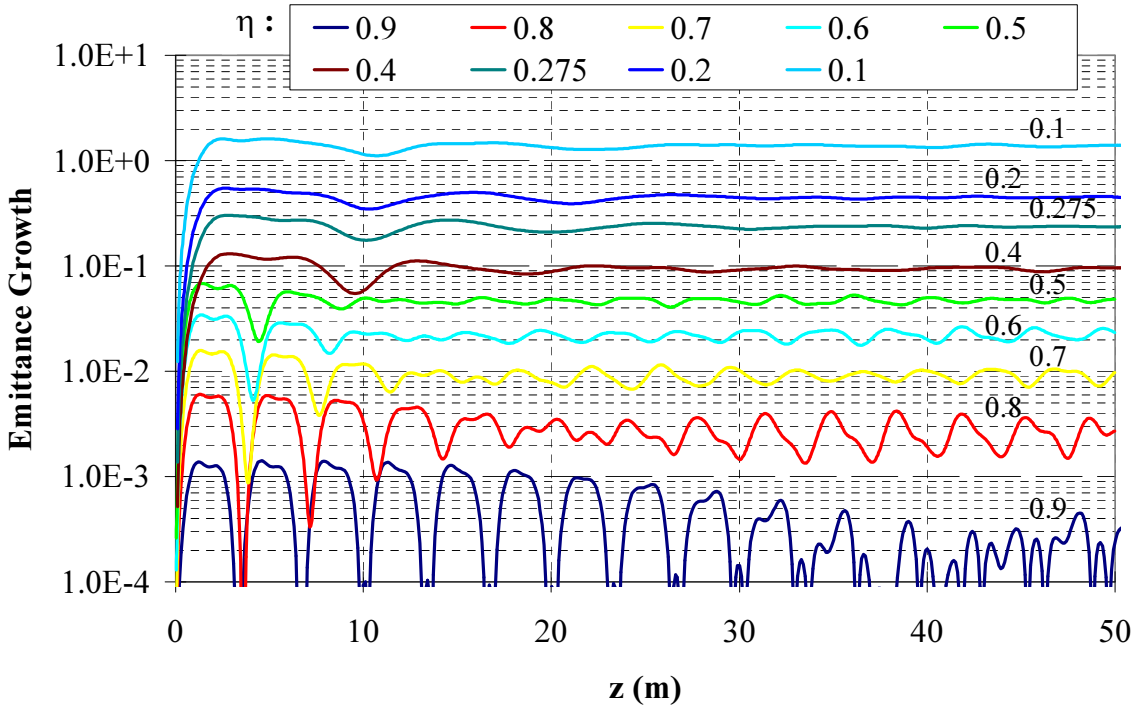

Figure 15 : Relative emittance growth of RMS-matched gaussian beams for different depress tune value (from 0.9 to 0.1).

The final relative emittance growth as well as the theoretical one given by formula (6.15) of [5] are represented on **Figure 16**. This formula gives the emittance growth induced by a difference of free energy between the gaussian beam and an homogenous one. The homogenous beam is assumed to be the final state of the beam. We now know that the final state equilibrium is an homogenous beam when the depress tune value is small, however with an edge which is never sharp. That is explaining why the curves are nearly the same at high current, but with a little difference coming from the edge-difference. At low current ($\eta \rightarrow 1$), the difference is large because the final equilibrium is not homogenous. The assumption of [5]: $a_f - a_i << a_i$, a_f and a_i being respectively the final and the initial effective beam radius, is verified in the simulations.

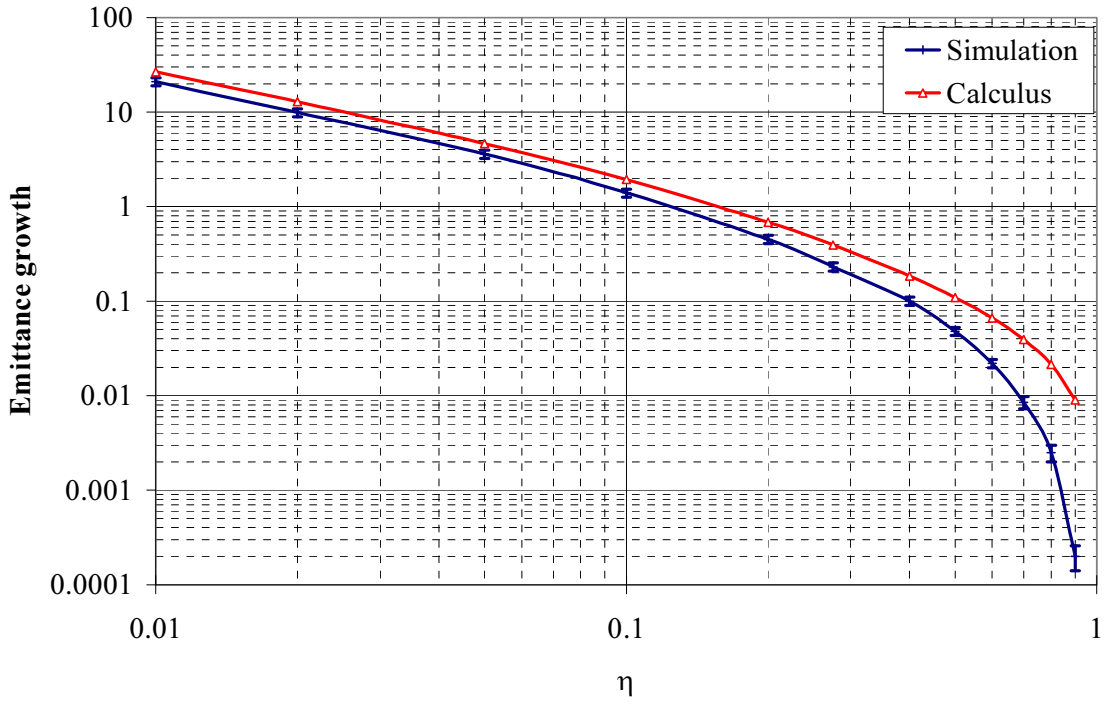

Figure 16 : Relative emittance growth at the end of the channel of RMS-matched gaussian beams with the depress tune.

2.2 Comparison between periodic and continuous channel

The problem involved in a real accelerator is the transport of a charged-particle beam through a periodic channel of period S. The evolution of the beam density distribution $f(\vec{r},\vec{p},t)$ is described by Vlasov's equation. Let us consider the equilibrium distribution $f_e(\vec{r},\vec{p},t)$ which has the same periodicity as the focusing channel :

$$f_e(\vec{r},\vec{p},t+T) = f_e(\vec{r},\vec{p},t)\,, \qquad \textbf{(Eq. 26)}$$

(T=S/v, v: particle velocity).

Integrating the Vlasov equation over one period yields:

$$\frac{1}{T}\int_t^{t+T}\frac{\partial f_e}{\partial t}dt = f_e(t+T) - f_e(t) = \frac{1}{T}\int_t^{t+T}\left(\vec{p}\cdot\vec{\nabla}_{\vec{r}} f_e + \frac{\vec{F}}{m}\cdot\vec{\nabla}_{\vec{p}} f_e\right)dt = 0\,, \qquad \textbf{(Eq. 27)}$$

then

$$\left\langle \frac{\vec{p}}{\gamma m}\cdot\vec{\nabla}_{\vec{r}} f_e + \vec{F}(\vec{r},t)\cdot\vec{\nabla}_{\vec{p}} f_e \right\rangle_T = 0\,, \qquad \textbf{(Eq. 28)}$$

The distribution $f_e(\vec{r},\vec{p},t)$ can be defined as the sum of the stationary distribution f_0 and a periodic perturbation δf_p, both transformed with a periodic linear transformation Rot according to the twiss parameter of the beam in the periodic channel :

(Eq. 29)

$$f_e(\vec{r},\vec{p},t) = \mathrm{Rot}\left(f_0(\vec{r},\vec{p}) + \delta f_p(\vec{r},\vec{p},t)\right).$$

We have then:

$$\frac{\vec{p}}{\gamma m}\cdot\vec{\nabla}_{\vec{r}} f_0 + \vec{F}(\vec{r},t)\cdot\vec{\nabla}_{\vec{p}} f_0 = 0 \text{ and } \left\langle \delta f_P(\vec{r},\vec{p},t)\right\rangle_T = 0 . \qquad \textbf{(Eq. 30)}$$

Function f_0 represents the stationary state of the beam distribution in the continuous focusing channel equivalent to the periodic channel. Equivalence means that both channels have the same mean focusing force, *i. e.*, the particles have the same phase advance per meter.

2.2.1 Beam density profile

Simulations in a FODO channel with $\sigma_0 = 60°$ phase advance per cell have been done. Quadrupole occupancy of the FODO channel is $\Omega = 0.5$ (quadrupole- as well as drift-lengths are ¼ of the lattice length).

Final density profiles of the beams, at the middle of a drift-space, have been represented on **Figure 17**. As in the continuous focusing channel, they exhibit a density-profile becoming more and more homogenous as the current increases. The central density of a space-charge dominated beam nearly reaches the one equivalent to the mean confinement force. The small difference (~8%) comes from that the average radius of the beam in a FODO channel is a little bigger than the one in its equivalent continuously focusing channel (in our case, for η=0.2, we have R_{FODO} = 8.9872 mm and R_{cont} = 8.6606 mm, which gives a relative radius difference of 3.8 %, and a relative transverse area difference of 7.7 %).

One's again, with small depress tune, the tails shape seem to have an exponential slope rather than gaussian as it is at low current.

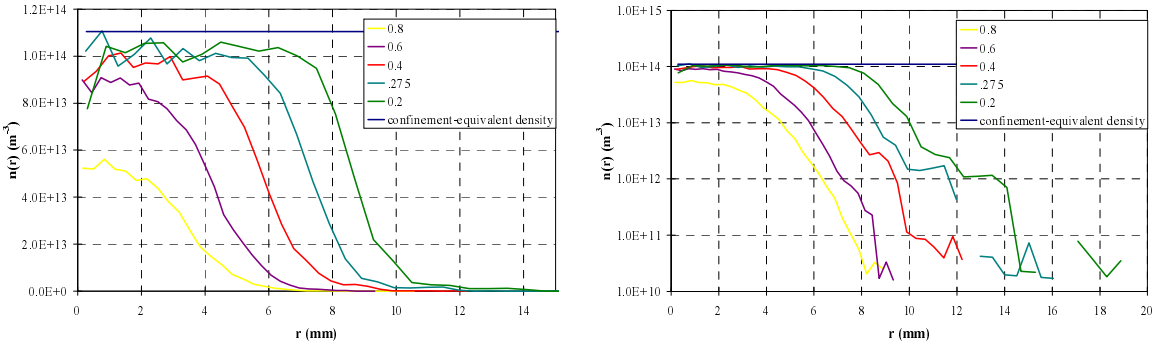

Figure 17 : Beam density-profiles at the end of the FODO channel (middle of drift)
Left : Linear scale. Right : Logarithm scale.

2.2.2 Beam phase-space distribution

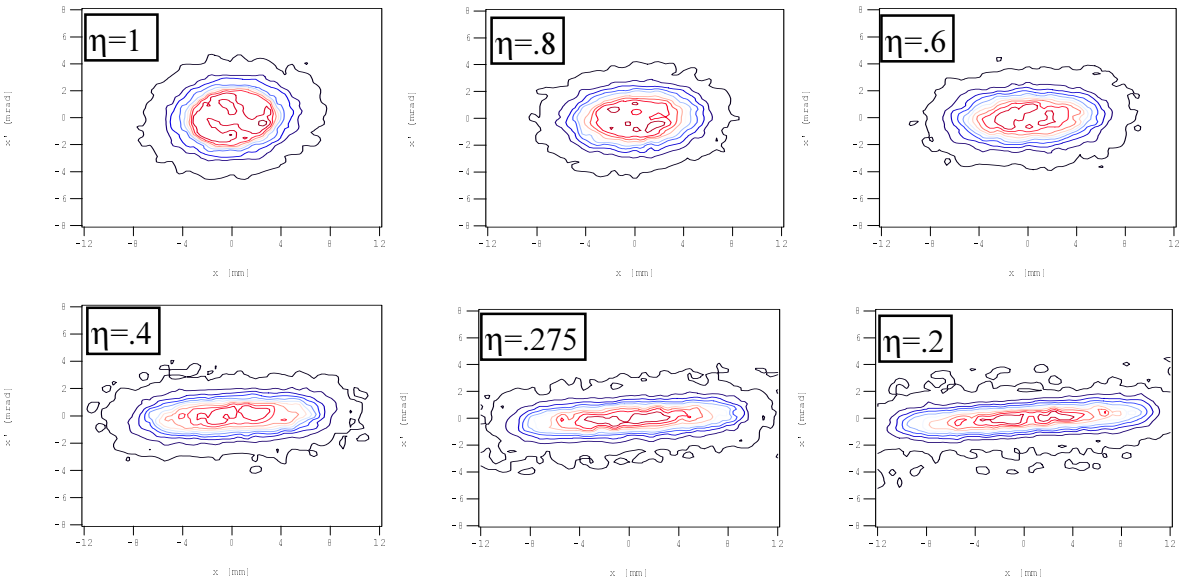

Figure 18 : Beam distribution in (x,x') phase-space at the end of a 20 meters FODO channel (middle of a x-focusing quad))for different tune depression.

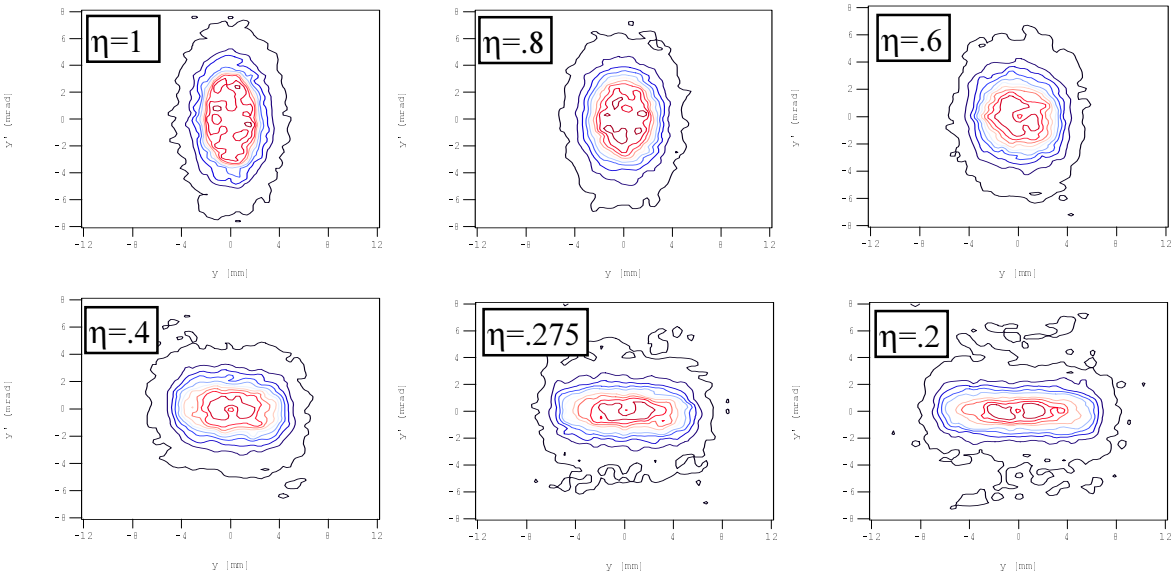

Figure 19 : Beam distribution in (y, y') phase-space at the end of a 20 meters FODO channel (middle of a x-focusing quad) for different tune depression.

On Figure **18** and Figure **19** have been represented the beam contour-plot in (x, x') and (y, y') phase-spaces at the middle of a x-focusing quadrupole at the end of the FODO channel (at 20 m from the input). The lines correspond to iso-density from 1 % to 81 % with 10 %

step. As in the continuous focusing channel, phase-space distributions in the 2 transverse directions becomes more and more rectangular as the beam current increases.

We have then studied the evolution of the beam-aspect ratio α in phase space with the depress tune η. Parameter α have been calculated from **Figure 14**, **Figure 18** and **Figure 19** and are represented on **Table 2**.

As represented in **Figure 20**, the beam-aspect ratio α of phase-spaces are the same in (x,x') or (y,y') in FODO or continuous channel. Evolution of α with η is very similar to the one obtained in **Figure 8**. One should pointed out that it is not representing exactly the same thing: on **Figure 8**, the hamiltonian-distribution was kept the same with a change of η, as in the case of **Figure 20**, the emittance is (nearly) the constant parameter.

η	*1.0*	*0.8*	*0.6*	*0.4*	*0.275*	*0.2*
α_x **(FODO)**	1	1.13	1.26	1.35	1.55	1.62
α_y **(FODO)**	1	1.10	1.27	1.35	1.52	1.61
$<\alpha>$ **(FODO)**	1	1.115	1.265	1.35	1.535	1.615
α **(Continuous)**	1	1.13	1.29	1.37	1.52	1.63

Table 2 : Beam-aspect ratio α with the depress tune η in continuous and FODO channel

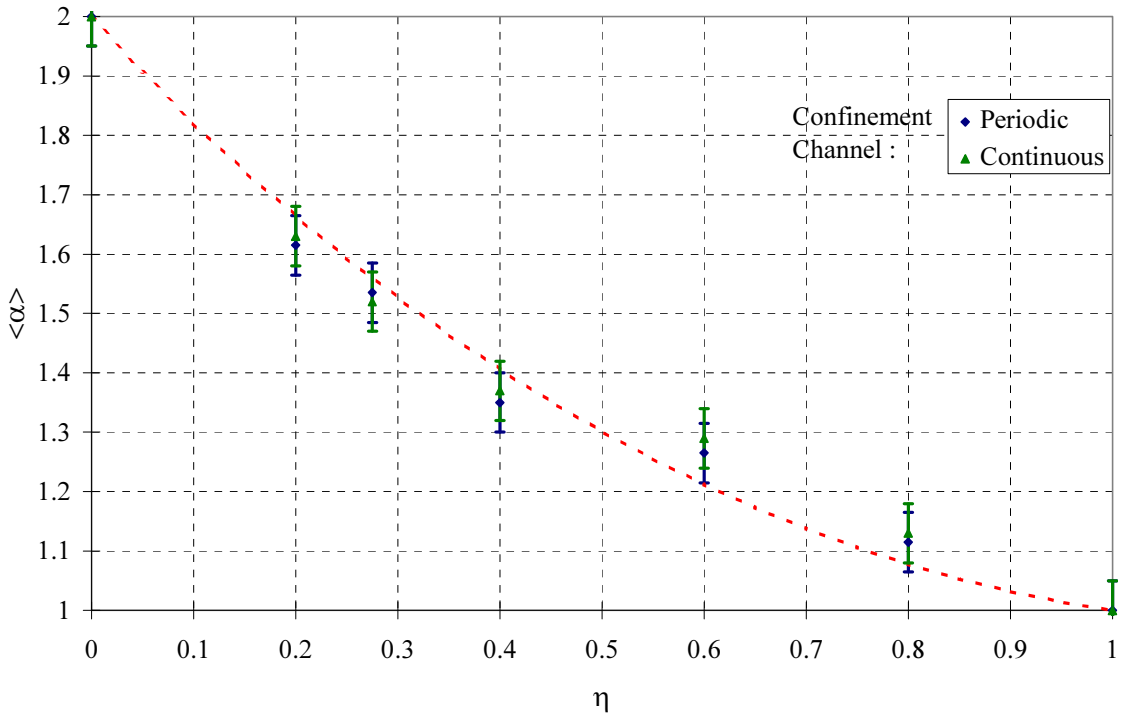

Figure 20 : Beam-aspect ratio α with the depress tune η in continuous and FODO channel

2.2.3 RMS emittance evolution

On **Figure 21**, is represented evolution of the rms-emittance in the continuous and the FODO channel. The space-charge depress-tune is 0.2, the initial beam distribution is gaussian.

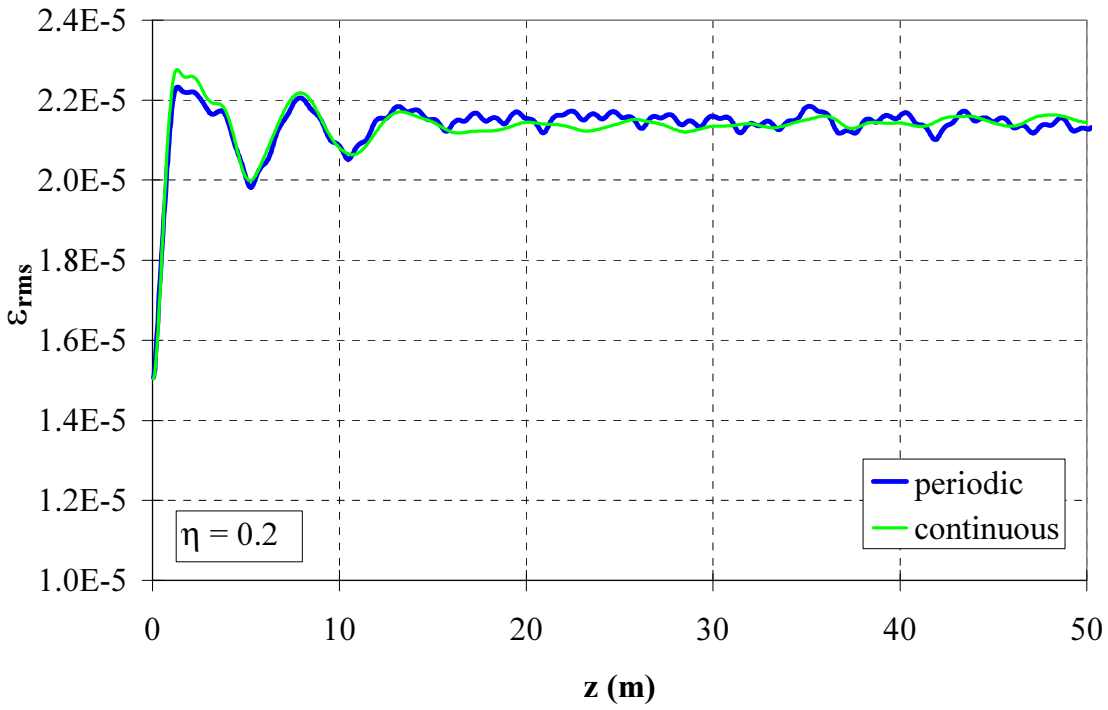

Figure 21 : RMS Emittance evolution in the continuous and FODO channel

The emittance evolution is the same (neglecting fluctuations) in the continuous and the FODO channel.

2.2.4 Evolution of the outermost particles

We have then studied the evolution of the beam radius normalised to the RMS size $\left(=\sqrt{\left(X/X_{rms}\right)^2+\left(Y/Y_{rms}\right)^2}\right)$ containing 90%, 99%, 99.9% and 99.99% of the particles. This has been done in a continuously focusing channel as well as FODO channels with σ_0 = 60° and 80° phase advance per cell (keeping the same phase advance per meter k_0 = 1 m^{-1}). The depressed tune is η = 0.2. The results are presented on **Figure 22**.

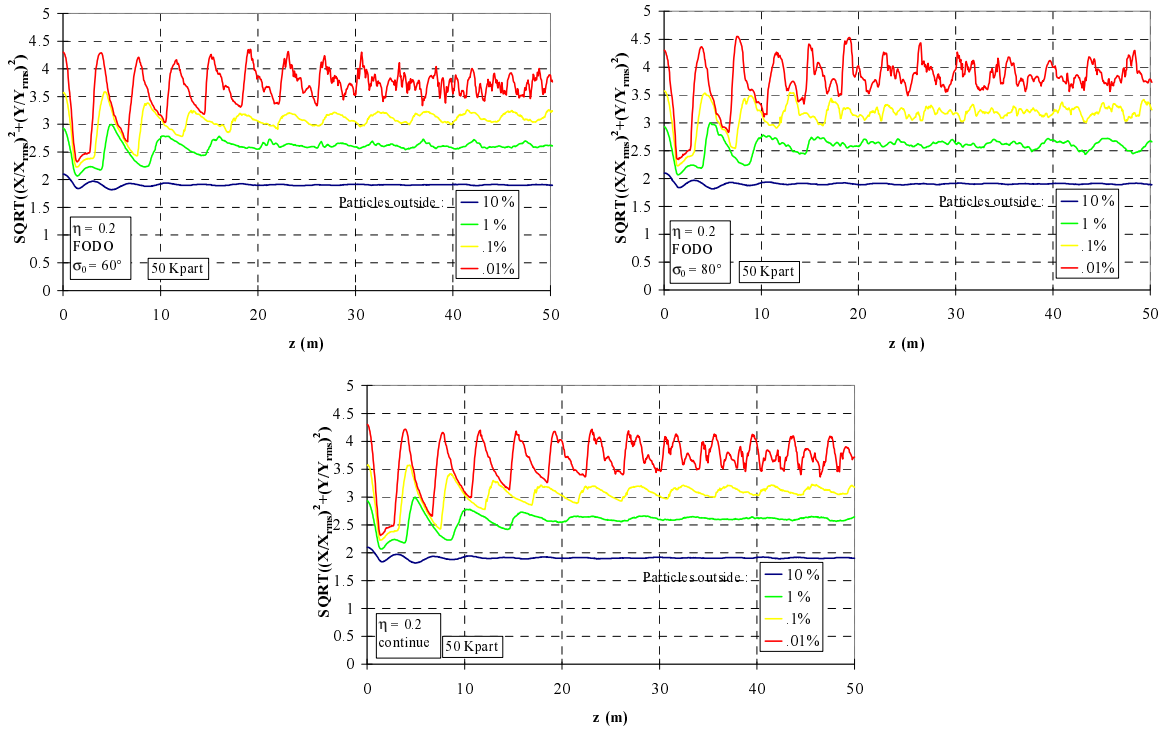

Figure 22 : Beam-dimensions evolution

a) FODO channel with $\sigma_0 = 60°$,

b) FODO channel with $\sigma_0 = 80°$,

c) Continuous channel

The continuously focusing channel seems to be a good model of a FODO channel even with large (80°) zero current phase advance per cell. Of course we already know that it is not the case when $\sigma_0 > 90°$, which induces a large emittance growth [5].

2.2.5 Conclusion on the comparison

The beam equilibrium in a periodic and its equivalent continuous channels seems to be the same as well for the core distribution as for the outermost (halo) particles. The smooth approximation seems to be very efficient in order to determine main beam characteristics.

2.3 Experimental results

The beam density profile and phase-space distribution of a 500 keV, up to 50 mA proton beam at the exit of a 29 period FODO channel have been measured using pepper-pot and scintillating screen looked by a intensified CCD camera [6].

In **Table 3**, has been represented the value of parameter $\zeta = \frac{K \cdot x_{RMS}^2}{4 \cdot \varepsilon_{RMS}^2}$ (which represents the ration between space-charge and emittance force) and of depress tune η for different beam currents.

I (mA)	0	10	30	50	100
$\langle x_{RMS} \rangle$ (mm)	1,5	1,8	2,6	3,1	4,2
ζ	0	1	6	15	55
η	1	.707	.378	.25	.134

Table 3 : ζ and η parameters with beam current.
(ε_{rms} = 3,75 π.mm.mrad)

2.3.1 Simulations

Transport simulation trough the FODO channel has been done with the 2D-MONET code with the space-charge routine SymEll (assuming a beam elliptical symmetry in transverse plan).

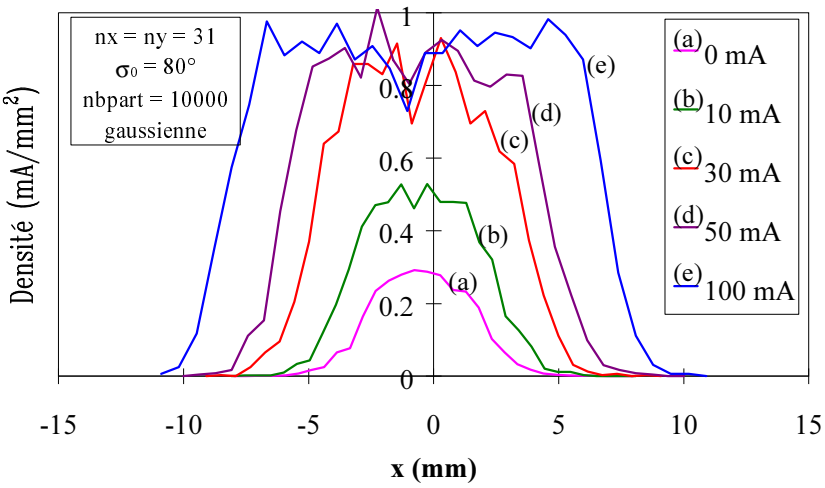

Figure 23 : Transverse beam profile at the middle of the last quadrupole for various beam current.
The phase advance per period without space-charge is σ_0=80°,
Gaussian (Left) and K-V (right) input matched beam.

On **Figure 23**, have been represented the transverse beam profiles at the middle of the last quadrupole for various beam current (from 0 to 100 mA). Initial gaussian and K-V beams are rms-matched to the channel. Output density profile of the initial gaussian beam tends to become homogenous as the current increases. At low current, the final distribution looks like the initial one. Same evolution is observed in vertical direction.

On **Figure 24**, have been represented the output phase-space distributions of the initial gaussian beam. The beam density in (x, y) seems to be uniform whatever the initial transverse energy of the beam. Notice : The initial total (kinetic + potential) energy of particles is correlated to particle colour and increases from red to blue. The distribution in (x', y'),

representing the particle kinetic energy, shows a redistribution of kinetic energy in the beam : Particles having the greatest total energy at input have the greatest kinetic energy at output, as can be deduced from the hollow output distributions shown on **Figure 25**, as the initial ones were not (**Figure 26**). The initial excess of potential energy has been transformed to kinetic one.

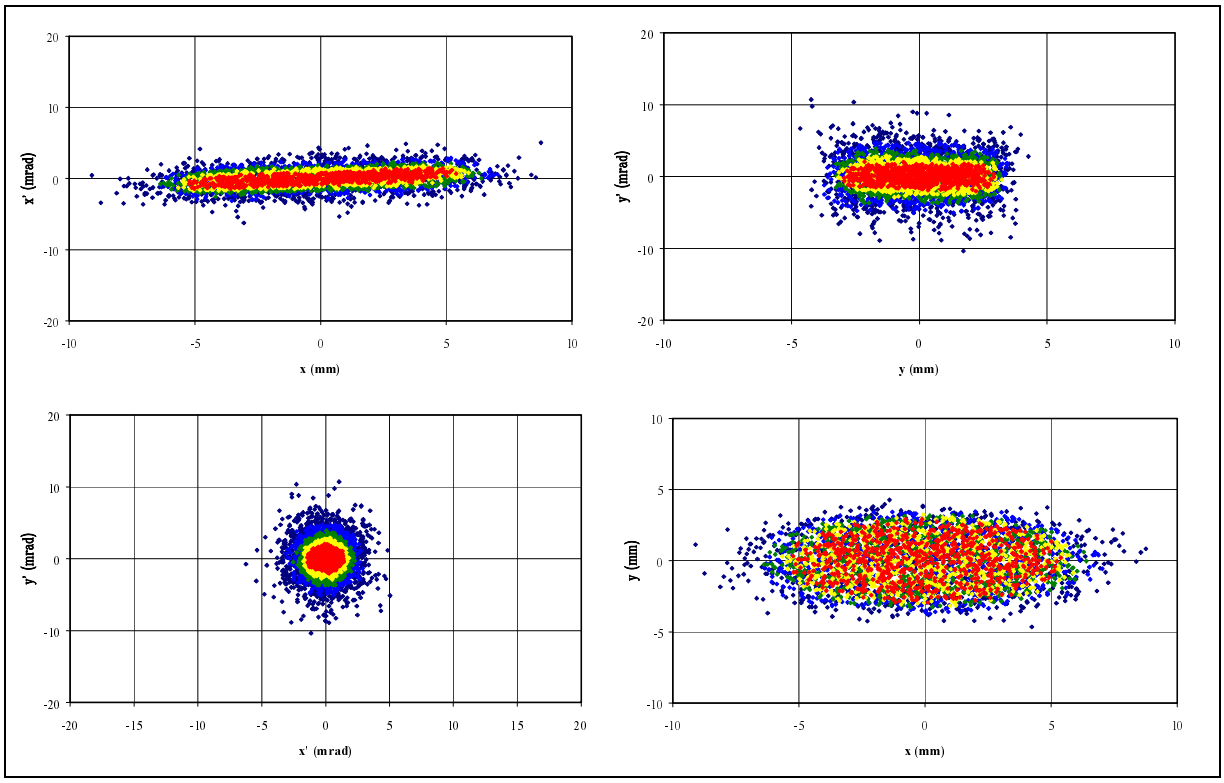

Figure 24 : Output phase-space distribution of a 50 mA, initially gaussian beam.

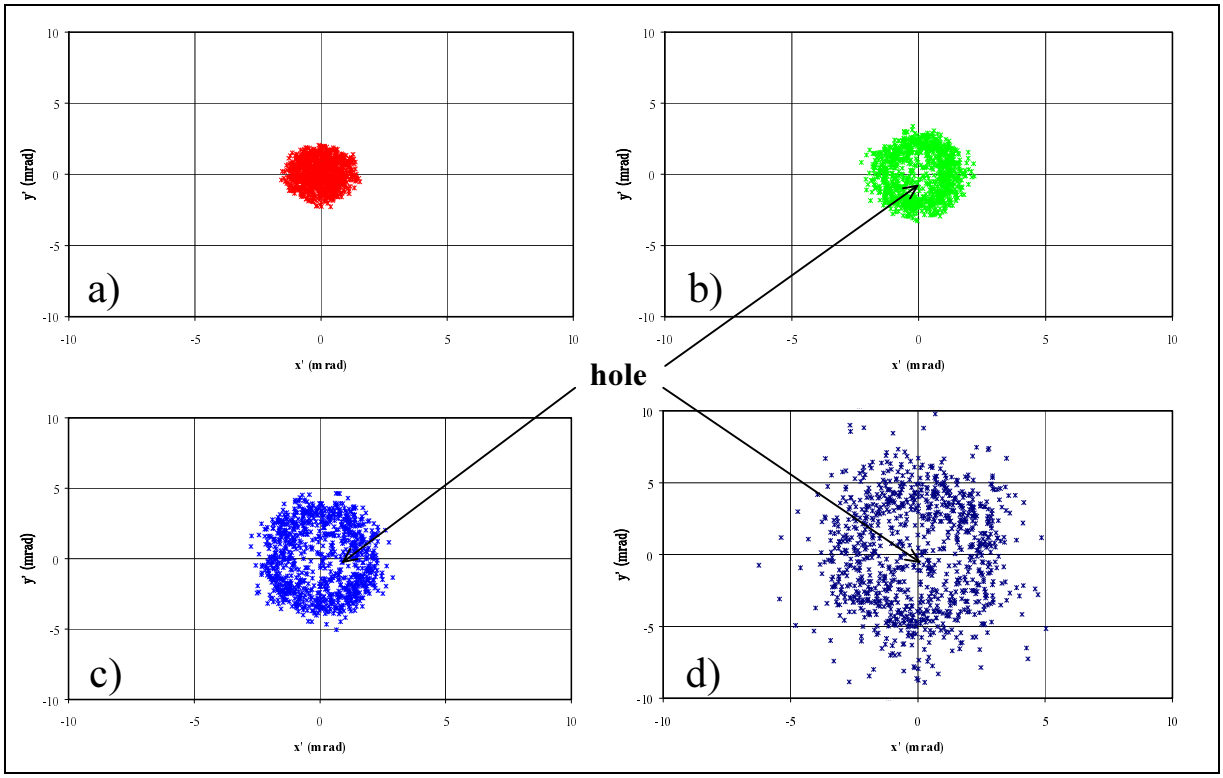

Figure 25 : Output (x', y') distribution of a 50 mA, initially gaussian beam.

a) ¼ of particles having the lowest input total energy,

b) ¼ of particles having the lowest input total energy greater than this of a),

c) ¼ of particles having the largest input total energy lower than this of d),

d) ¼ of particles having the largest input total energy.

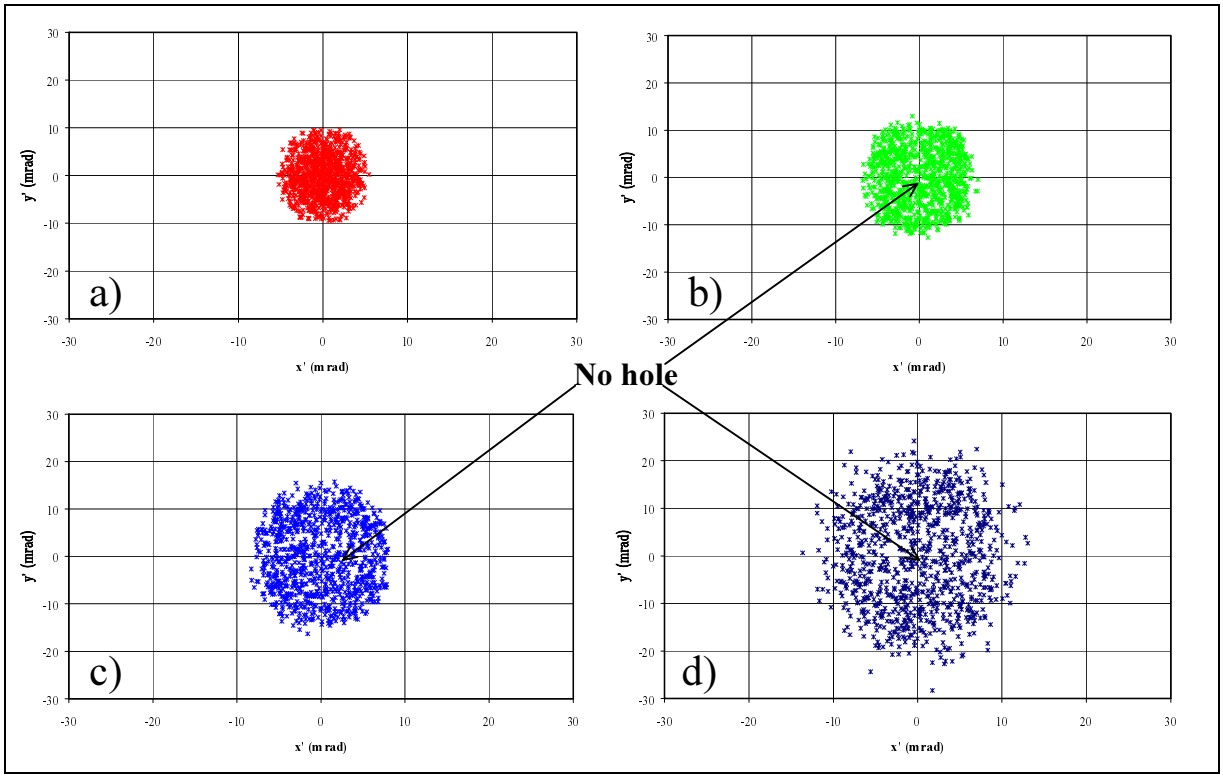

Figure 26 : Inputt (x', y') distribution of a 50 mA, initially gaussian beam.

a) ¼ of particles having the lowest input total energy,

b) ¼ of particles having the lowest input total energy greater than this of a),

c) ¼ of particles having the largest input total energy lower than this of d),

d) ¼ of particles having the largest input total energy.

2.3.2 Experimental measurements

The phase advance per period used is 60°. The measurement of the beam distribution at the channel input has been done with the sampling hole method [7]. Output measurement have been done with the pepper-pot method and imaging technics [7].

The beam has been first measured and matched to the channel for various intensities (from 2,2 to 37 mA). On **Figure 27**, have been presented the (x, x') beam distributions measured at the source exit.

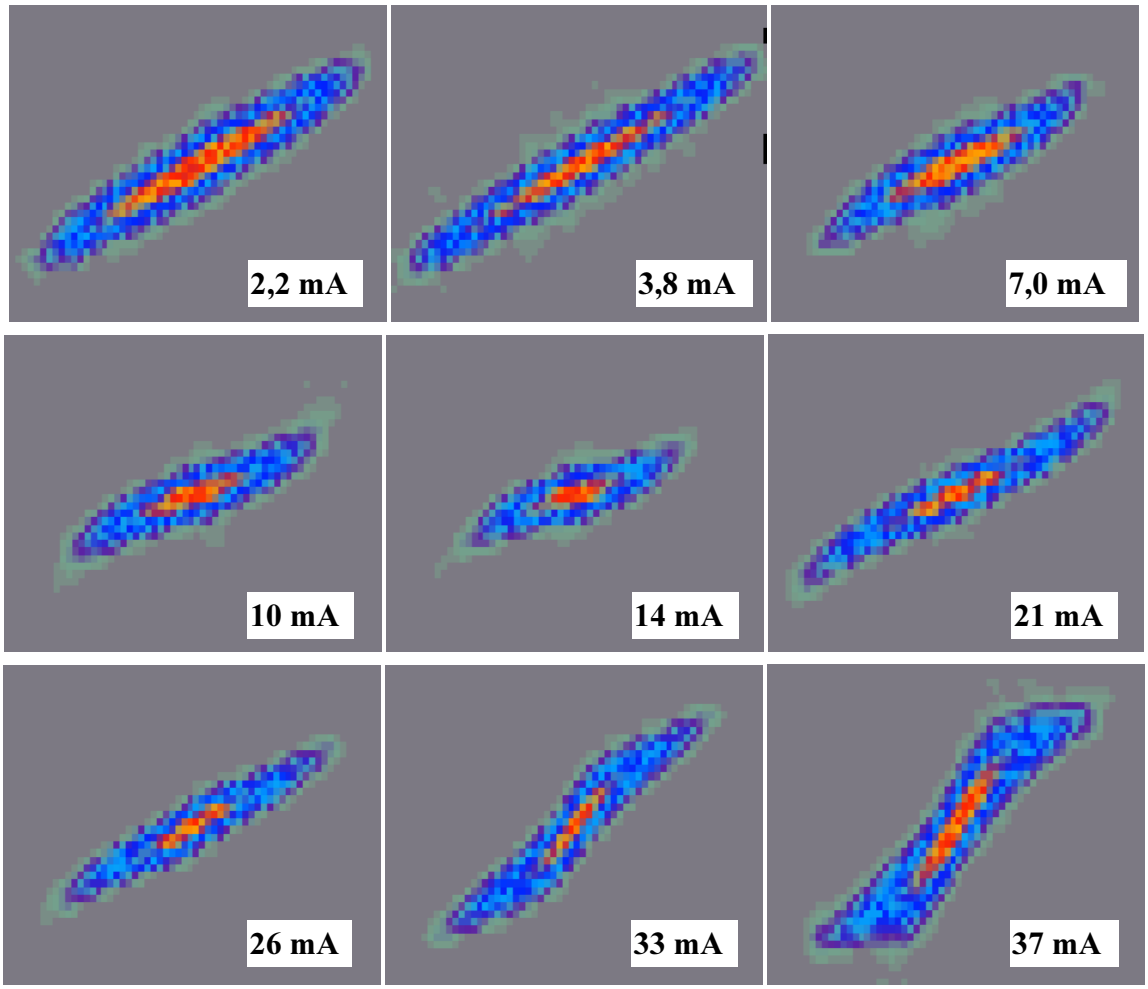

Figure 27 : (x, x') beam distributions measured at the source exit.
Full scale is 30 mm, 20 mrad.

From the distribution of **Figure 27** have been obtained the beam density profile at the source exit (**Figure 28**). These profiles are very similar whatever the beam current. They are far from homogenous.

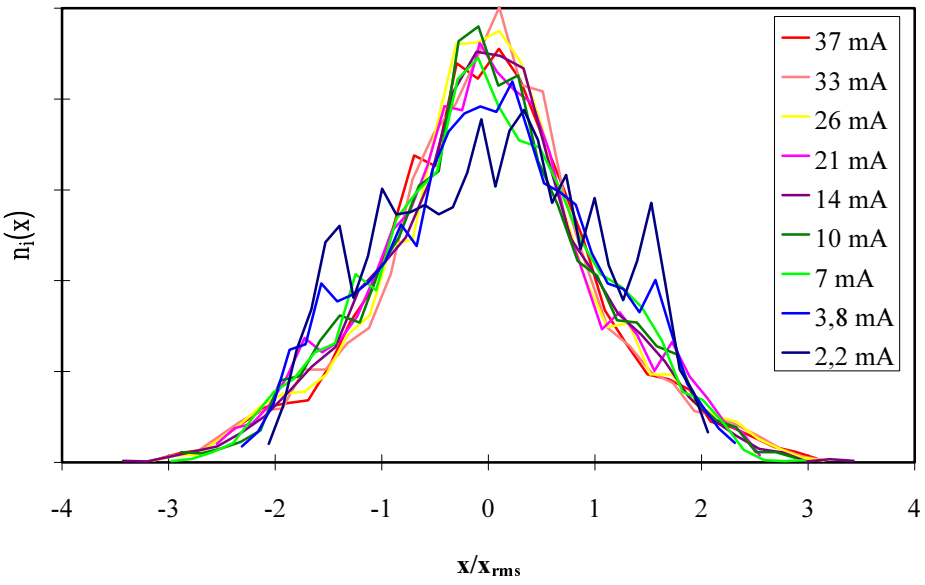

Figure 28 : Beam density profile at the source exit

Channel-output beam profiles have been then measured and are represented on **Figure** 29.

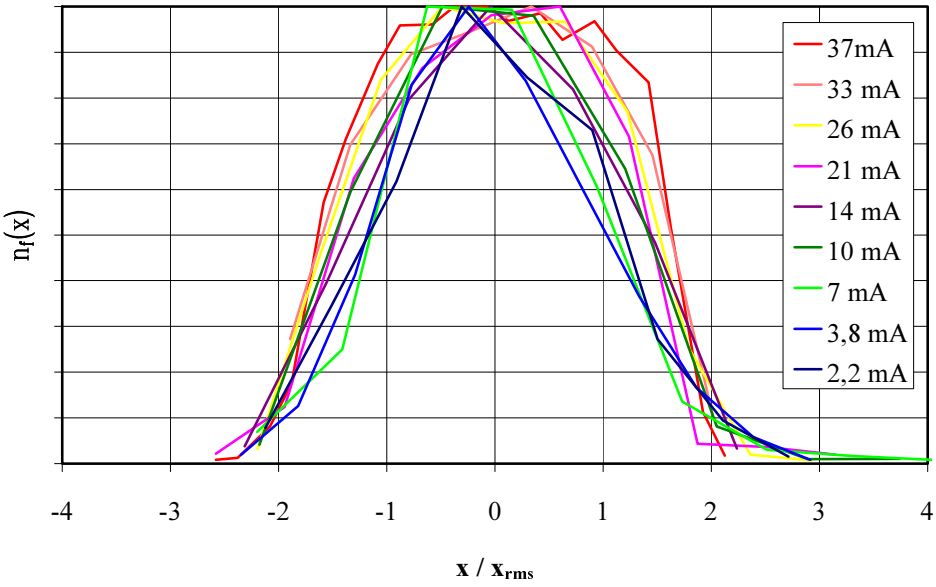

Figure 29 : Beam density profile at the channel output

The higher the beam current is, the more homogenous the beam density profile at the output of the FODO channel is. The beam has reached a new equilibrium before the channel's end (as shown in the simulations).

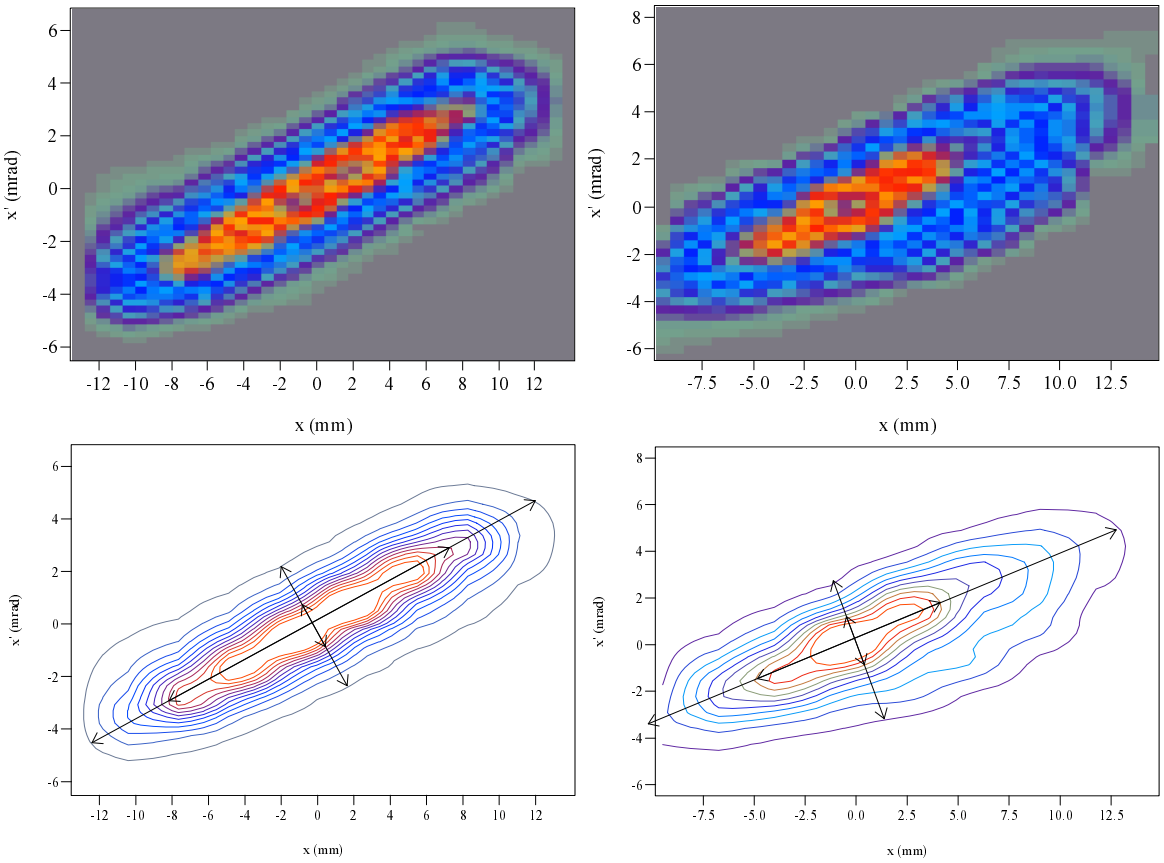

Figure 30 : Beam phase-space distribution at the exit of the FODO channel for a beam current of 37 mA (left) and 2,2 mA (right)

On **Figure 30**, has been represented the (x, x') phase-space distribution at the FODO output. It has been measured with the pepper-pot method.

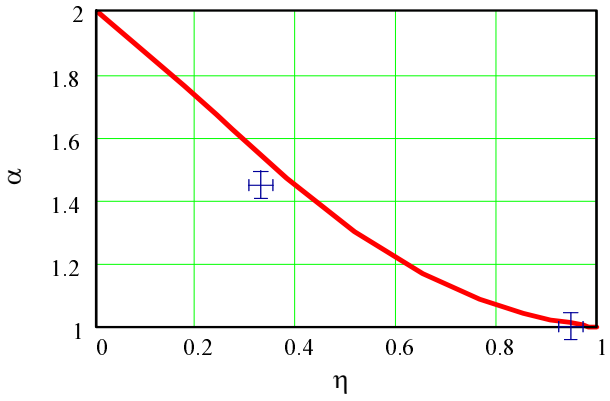

Figure 31 : Evolution of the α parameter as a function of the depress tune η.
Cross : experimental measurement,
Curve : Water-bag beam.

The α parameter has then been calculated for this two different beam current. They have been included on **Figure 31**, and compared with the water-bag case.

The beam equilibrium shape observed experimentally agrees very well with the one found theoretically.

3. Summary

Six very different stationary distributions of unbunched beams have been semi-analytically studied by solving the Vlasov-Maxwell system in a linear continuous focusing channel. It has been observed that:

- Density profile of stationary distributions becomes uniform when the beam is space-charge dominated,
- Beam distribution in 2D phase-space becomes rectangular as space-charge increases.

An expression of the beam border width has been found, and a model given the halo-particles trajectories in phase-space around a space-charge driven beam has been created. This model will be of great use to determine the space-charge influence on halo from intrabeam scattering or scattering on residual gas.

Simulations have shown the good equivalence between periodic and continuous confinement channels in term of beam stationary distributions, emittance and halo evolution. An experiment, aiming to measure the stationary distribution of a space-charge driven proton beam in a FODO channel, has given the predicted as well with the semi-analytic model in continuous focusing channel as with simulations. The use of continuous channel in halo studies, which considerably reduces difficulties, has then be justified.

References

[1] F. J. Sacherer, *RMS Envelope Equation with Space-charge*, IEEE Trans. Nucl. Sci., **NS 18**, 1105 (1971).

[2] N. Pichoff, *Intrabeam Scattering on Halo Formation*, Note DAPNIA/SEA 98/46, 1998.

[3] N. Pichoff, *Halo Formation from Halo Scattering of Beam Particles on Residual Gas*, Note DAPNIA/SEA 98/45, 1998.

[4] N. Pichoff, *Etude Théorique et Expérimentale du Halo d'un Faisceau Intense de Particules Chargées dans un Accélérateur*, Ph.D. report, December 1997.

[5] M. Reiser, *Theory and Design of Charged Particles Beam*, J. Wiley & Son, Editor, 1994.

[6] N. Pichoff et al., *Transverse profile equilibrium in a space-charge dominated beam*, Proc. of the 1st Asian. Part. Accl. Conf., APAC98 (1998).

[7] G. Haouat et al., *Measurements of initial beam conditions for halo formation studies,* EPAC 96, Sitges (Barcelona), Spain, June 10-14, 1996.